Available online at www.sciencedirect.com
ScienceDirect
Journal of Solid State Chemistry 180 (2007) 3551–3559
JOURNAL OF SOLID STATE CHEMISTRY
www.elsevier.com/locate/jssc

Controllable synthesis of $NiC_2O_4 \cdot 2H_2O$ nanorods precursor and applications in the synthesis of nickel-based nanostructures

Wei-Guo Tian[a,b], Pan-Pan Wang[a,b], Ling Ren[a,b], Gen-Ban Sun[c], Ling-Na Sun[a,b], Kai Yang[a,b], Bing-Qing Wei[d,**], Chang-Wen Hu[a,b,*]

[a]*Department of Chemistry, Institute for Chemical Physics, Beijing, China*
[b]*State Key Laboratory of Explosion Science and Technology, Beijing Institute of Technology, Beijing 100081, PR China*
[c]*College of Chemistry, Beijing Normal University, Beijing 100875, PR China*
[d]*Department of Mechanical Engineering, University of Delaware, Newark, DE 19716, USA*

Received 3 July 2007; received in revised form 4 September 2007; accepted 29 September 2007
Available online 13 October 2007

Abstract

A controllable synthesis of $NiC_2O_4 \cdot 2H_2O$ nanorods precursor was obtained via the microemulsion-mediated solvothermal method and a further synthesis of β-$Ni(OH)_2$ nanorods, nickel oxide (NiO) sub-microtubes, Ni nanospheres and flower-like nickel complexes nanostructures by using the precursor. The morphologies and crystalline structures were characterized by scanning electron microscopy (SEM), transmission electron microscopy (TEM), selected area electron diffraction (SAED), and the X-ray powder diffraction (XRD). The morphologies and sizes of the precursors can be readily tuned by adjusting experimental parameters of the reverse microemulsion system. The synthesized β-$Ni(OH)_2$ nanorods composed of fine nanosheets shown excellent electrochemical performance as an electrode material in rechargeable battery systems.

Keywords: Microemulsion system; Solvothermal; Precursor; Specific capacity

1. Introduction

Low-dimensional nanomaterials of nickel and its compounds have been extensively studied owing to their widespread applications in catalysis [1,2], electronics [3], magnetics [4–8], etc. For instance, nickel hydroxide ($Ni(OH)_2$) has been applied in alkaline rechargeable batteries [9–11]. While nickel oxide (NiO) is a semiconductor and antiferromagnetic material and is also used in diverse fields, such as catalysis, gas sensors, electrochromic films, magnetic materials, active optical fibers, and fuel cell electrodes [12–15]. Recently, Taeghwan et al. [16] have demonstrated the synthesis of NiO-coated Ni nanoparticles and their successful application in the magnetic separation of His-tagged proteins. So far, many methods have been developed to fabricate nanostructured materials, among which using precursor is one of the successful methods. The precursor methods have been deeply developed to fabricate nickel nanostructures. Wang et al. [17] have reported the synthesis of NiO nanowires by oxygenating NiS nanoparticles. Qi et al. [18] have prepared Ag cage by reducing Ag_3PO_4 rhombododecahedral crystals. Li et al. [19] have synthesized $Ni(OH)_2$ coexistence of nanosheets and nanorods via bulk nickel oxalate NiC_2O_4 in NaOH solution at 160 °C for 12 h. Wang et al. [20] have successfully prepared NiO nanowires via the decomposition of NiC_2O_4 at high temperature. Therefore, how to prepare a suitable precursor becomes a crucial factor to obtain ideal building blocks for synthesizing different nanostructured materials. Among all the methods, the reverse micelles or microemulsion system have already been widely used to prepare different nanostructured materials. In our group, we have successfully prepared BaF_2 nanowhiskers [21], ultra-high-aspect-ratio $Ca_{10}(PO_4)_6(OH)_2$ nanofibers [22], MgF_2

**Also corresponding author.
*Corresponding author. State Key Laboratory of Explosion Science and Technology, Beijing Institute of Technology, Beijing 100081, PR China. Fax: +86 10 68914780.
E-mail addresses: weib@udel.edu (B.-Q. Wei), cwhu@bit.edu.cn (C.-W. Hu).

0022-4596/$ - see front matter © 2007 Elsevier Inc. All rights reserved.
doi:10.1016/j.jssc.2007.09.036

nanorods [23], $SrCO_3$ and $SrWO_4$ nanostructures with various morphologies [24,25] by the microemulsion-mediated solvothermal method.

In this article, we report a controllable synthesis of $NiC_2O_4 \cdot 2H_2O$ nanorods precursor via microemulsion-mediated solvothermal method. The morphologies and sizes of the precursor can be readily tuned by adjusting experimental parameters of the reverse microemulsion system, such as the molar ratio of H_2O to CTAB (defined w), the reaction temperature (T) and time (t). Furthermore, we have successfully demonstrated that β-$Ni(OH)_2$ nanorods composed of nanosheets, NiO sub-microtubes, Ni nanospheres and flower-like nickel complexes assembled by nanorods can be synthesized by using $NiC_2O_4 \cdot 2H_2O$ nanorods as precursor which has not been reported before. In addition, we have studied the electrochemical performance of β-$Ni(OH)_2$ electrode.

2. Experimental section

2.1. Materials

All chemicals, nickle sulfate ($NiSO_4 \cdot 6H_2O$, 99%), oxalic acid ($H_2C_2O_4 \cdot H_2O$, 99%), sodium hydroxide (NaOH), cetyltrimethylammonium bromide (CTAB), cyclohexane (C_6H_{12}), *n*-pentanol ($C_5H_{12}O$), and hydrazine hydrate ($NH_2NH_2 \cdot H_2O$, 50%) (Beijing Chemical Reagent, Co.) are analytical grade and were used without further purification distilled and deionized water was used in all of the studies.

2.2. Preparation of $NiC_2O_4 \cdot 2H_2O$ nanorods precursor

First, two same quaternary micromulsion systems, CTAB/water/cyclohexane/*n*-pentanol, were prepared by dissolving 5 mmol CTAB in 30 mL of cyclohexane and 1.5 mL of *n*-pentanol. The mixing solution was stirring for 30 min until it became transparent. And then, $NiSO_4$ and $H_2C_2O_4$ aqueous solutions of identical concentration and volume were added to the above microemulsion solutions, respectively. After substantial stirring, the two optically transparent microemulsion solutions were mixed together and stirred for another 10 min. The resulting microemulsion solution was then transferred into an 80 mL stainless Teflon-lined autoclave and heated at 120 °C for 12 h. After the reaction was completed, the resulting suspension was naturally cooled to the room temperature, and the precipitates were collected by centrifuging, washed for several times with absolute ethanol and distilled water, and dried in atmosphere at the room temperature.

2.3. Synthesis of β-Ni(OH)$_2$ nanorods, NiO submicortubes, Ni nanospheres and flower-like nickel complexes

In a typical synthesis process, 2 mmol of the $NiC_2O_4 \cdot 2H_2O$ nanorods precursor and 4 mL 1 M NaOH were dispersed in 50 ml distilled water successively. The suspension was heated up to boil for 30 min by vigorously stirring under atmosphere condition. Then the resultant green precipitates were naturally cooled to the room temperature. The precipitates were collected by centrifuging and washed with absolute ethanol and distilled water for several times, and then dried in atmosphere at the room temperature.

Meanwhile the NiO sub-microtubes were obtained by calcination of the as-prepared $NiC_2O_4 \cdot 2H_2O$ nanorods at 400 °C for 2 h in a Muffle furnace.

The Ni nanospheres were prepared by reducing $NiC_2O_4 \cdot 2H_2O$ nanorods precursor with $NH_2NH_2 \cdot H_2O$. Firstly, 0.5 mmol of the precursor $NiC_2O_4 \cdot 2H_2O$ nanorods was dispersed in 50 mL distilled water, then added 1 mL 1 M NaOH and 10 mL $NH_2NH_2 \cdot H_2O$ orderly. The resulting suspension was then transferred into an 80 mL stainless Teflon-lined autoclave and heated at 120 °C for 12 h. The resultant black precipitates were naturally cooled to the room temperature, then collected, washed with ethanol and water for several times, and dried in vacuum. However, when we changed the hydrothermal treatment to an ultrasonic treatment at 70 °C for 6 h and kept the other condition invariable, we finally obtained the violet mixture of flower-like nickel complexes assembled by nanorods.

2.4. Characterizations

The overall crystallinity and purity of the as-synthesized samples were analyzed by X-ray powder diffractometer (XRD) equipped with graphite monochromatized Cu$K\alpha$ radiation ($\lambda = 1.54060$ Å) by a SHIMADZU XRD-6000 operated at 40 kV voltage and 50 mA current. XRD patterns were recorded in the 2θ range of 10–80° with a scanning step of 0.02°. The thermogravimetric analysis (TGA) of $NiC_2O_4 \cdot 2H_2O$ was carried out on Perkin Elmer Diamond TG-DTA/DSC apparatus (Germany) with a heating rate of 10 °C min^{-1} in flowing air from 80 to 900 °C. The morphology patterns, size distribution and selected area electron diffraction (SAED) of the as-prepared products were observed using Hitachi model H-800 transmission electron microscope (TEM), and S-4800 scanning electron microscope (SEM) at the accelerating voltage of 200 kV and 15 kV, respectively. The specimens for TEM images and SAED studies were prepared by suspending the solid samples in ethanol. About 1 mg of sample was added into 5 mL ethanol in a small glass container that was then placed in an ultrasonic water bath and sonicated for 15 min. A drop of this well-dispersed suspension was placed on a carbon-coated 200-mesh copper grid, followed by drying the sample under ambient condition before it was placed in the sample holder of the microscope.

2.5. Preparation of the β-Ni(OH)$_2$ electrode

The active material paste containing β-$Ni(OH)_2$ and nickel powder was inserted into a 1 cm × 1 cm nickel foam

using polytetrafluoroethylene (PTFE) as the binder agent. After drying at 60 °C for 2 h in vacuum, the above electrode was sandwiched between two identical Ni foam electrodes and pressed into a thickness of 0.5 mm as the work electrode at 20 MPa for 5 min. The β-$Ni(OH)_2$ electrode was immersed into the alkaline electrolyte containing 6.0 M KOH and 1.0 M LiOH, using a MH (hydrogen storage alloy) as the counter electrode and Hg/HgO (6.0 M KOH) as the reference electrode. The cell was then charged at 0.2 C (200 mA) for 6 h, rested for 1 h, and then discharged until the potential decreased to 1.0 V. The charge–discharge experiment was repeated until the discharge capacity became stable.

3. Results and discussion

3.1. Morphology discussion and possible formation mechanism of $NiC_2O_4 \cdot 2H_2O$ nanorods

Several experimental factors, which may have effects on the morphology of the synthesized precursor, such as the value of w (molar ratio of H_2O to CTAB), reaction temperature (T) and time (t), have been studied. Fig. 1 shows typical SEM and TEM images of the $NiC_2O_4 \cdot 2H_2O$ nanorods precursor prepared under different conditions. As shown in Fig. 1a, the precursor was prepared in the microemulsion system, with $NiSO_4$ and $H_2C_2O_4$ aqueous

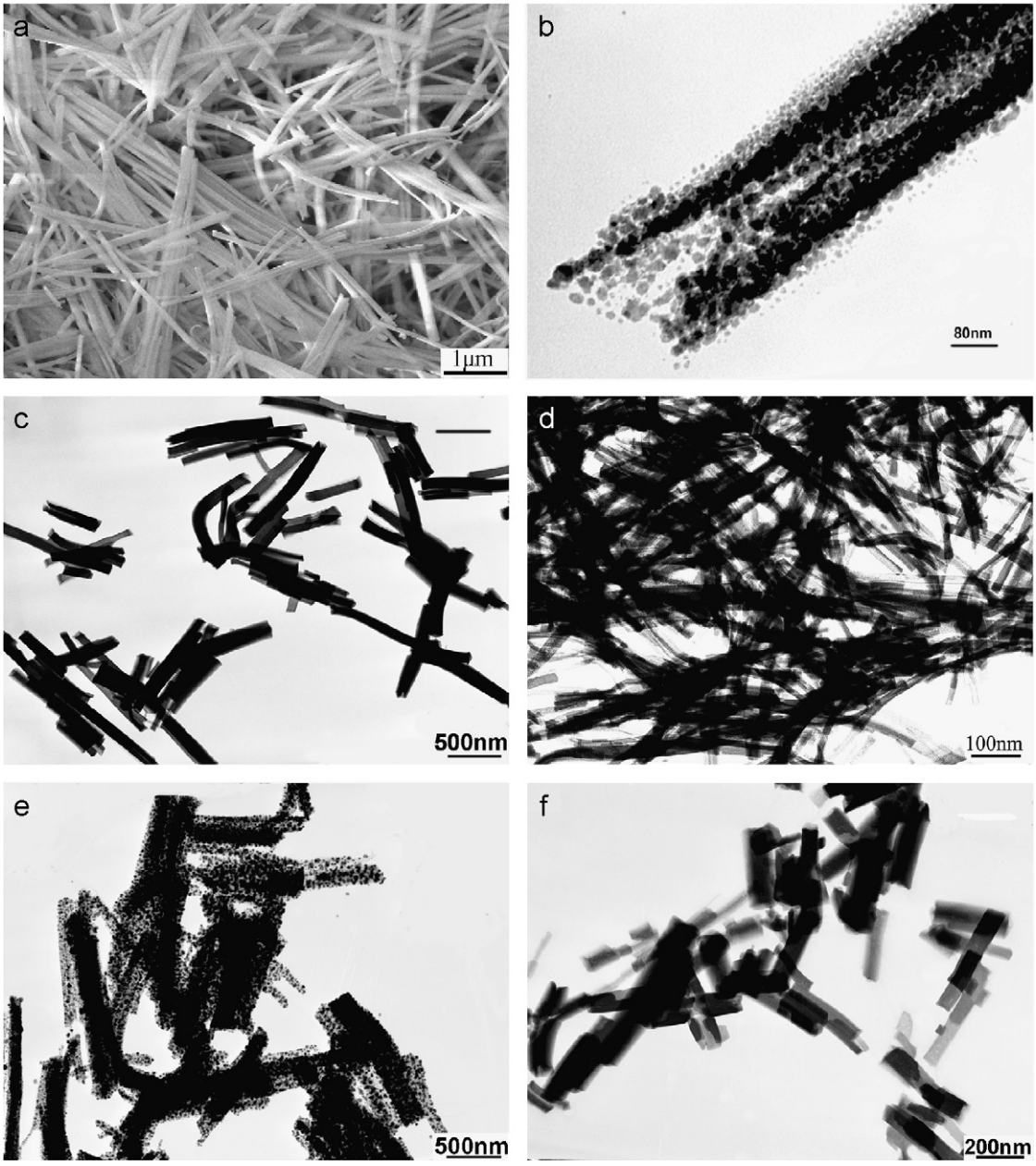

Fig. 1. SEM and TEM images of $NiC_2O_4 \cdot 2H_2O$ nanorods under different condition: (a) $w = 20$, $T = 120$ °C, $t = 12$ h; (b) the high magnification of (a); (c) $w = 10$, $T = 120$ °C , $t = 12$ h; (d) $w = 5$, $T = 120$ °C, $t = 12$ h; (e) $w = 20$, $T = 160$ °C, $t = 12$ h; (f) $w = 20$, $T = 120$ °C, $t = 6$ h.

solutions of identical concentration of 0.5 M and identical volume of 2 mL ($w = 20$) at 120 °C for 12 h. The precursor $NiC_2O_4 \cdot 2H_2O$ is composed of nanorods with diameters of about 200 nm and lengths up to 2 μm, and the nanorods are made up of large-scale naoparticles with size of 20 nm, as shown in Fig. 1b. In Fig. 1c and d, the precursor was prepared at $w = 10$ and 5, respectively, with other conditions invariable compared to Fig. 1a. The TEM images reveal that the diameters of the $NiC_2O_4 \cdot 2H_2O$ nanorods are 100 and 20 nm, with lengths up to 0.5–1 and 0.5 μm, respectively. It is obviously that the diameters and lengths become smaller and shorter with the decrease of the w value.

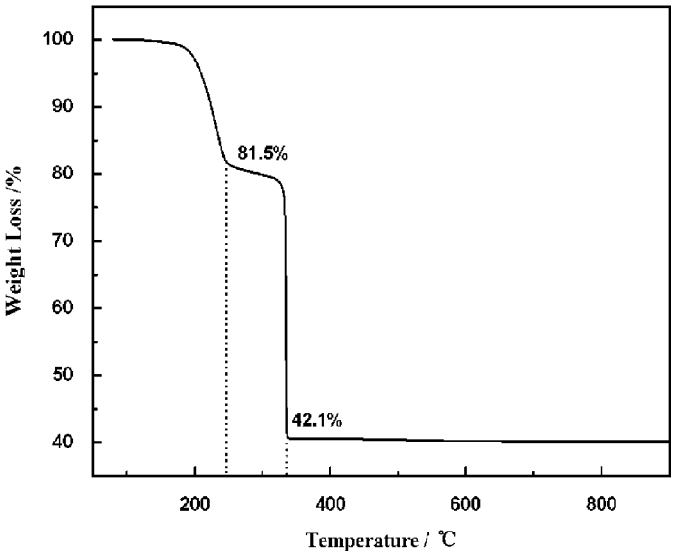

Fig. 2. TGA curve of $NiC_2O_4 \cdot 2H_2O$ nanorods.

The possible formation mechanism can be understood as following, similar to the preparation of BaF_2 nanofibers [21]. When two microemulsion solutions containing $NiSO_4$ and H_2CO_4 are mixed, $NiC_2O_4 \cdot 2H_2O$ nucleation and irreversible micellar fusion may occur at the same time. When the w value is low, the fuse rates between two spherical droplets will be very slow due to a small amount of exchangeable water molecules in the microemulsions, resulting in a short cylindrical droplet. Such a microemulsion droplet comprises a centrally located short rod-like $NiC_2O_4 \cdot 2H_2O$ nucleus with water enriched at both ends of the droplet. The CTAB molecules of the side surfaces of the cylindrical droplet may adsorb on the surface of the formed nucleus, and therefore these molecules are fixed and immobilized. In contrast, the CTAB molecules at both ends of the cylindrical droplet do not combine with the nucleus and are relatively free. Thus, the cylindrical microemulsion droplet may dynamically exchange with other microemulsions at both ends of the droplet. This process results in the formation of one-dimensional nanostructures. When the w value increases, the cylindrical droplet becomes bigger and longer. Thus, the diameters and lengths of the $NiC_2O_4 \cdot 2H_2O$ nanorods become bigger and longer when the w value increased.

When the reaction temperature increased from 120 to 160 °C, the average length was about 1.5 μm, slightly shorter but with the diameters remained almost the same, as shown in Fig. 1e. We speculated that the reaction speed becomes quicker and tends to form shorter nanorods to achieve stable shape with increase of temperature. While in Fig. 1f, when the reaction time decreased to 6 h, the diameters and lengths were about 100 nm and 0.3 μm, respectively. It is easy to understand that the reaction was not complete, resulting in smaller and shorter products.

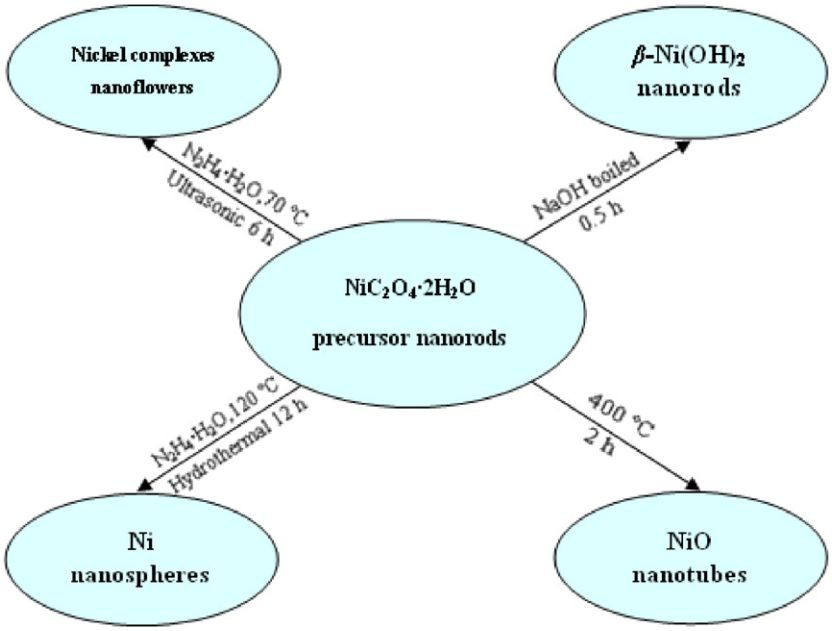

Scheme 1. All the reactions based on the precursor $NiC_2O_4 \cdot 2H_2O$ nanorods.

After comparing all of them, we found that the precursor's morphology was relative best and uniform without curving rods, which was obtained at $w = 20$, $T = 120\,^{\circ}C$ and $t = 12\,h$.

3.2. TGA analysis of the $NiC_2O_4 \cdot 2H_2O$ nanorods

The TGA curve of the $NiC_2O_4 \cdot 2H_2O$ nanorods precursor is shown in Fig. 2. There are two weight loss steps at the temperature in the ranges of 50–250 and 250–340 °C, respectively. The first weight loss is mainly attributed to the evaporation of H_2O, whereas the second one is ascribed to the decomposition of the anhydrous nickel oxalate. The weight losses are about 18.5% and 39.4%, which are close to the theoretical value of 19.7% and 40.0%, respectively. Thus, we can surely confirm that there are two crystal water molecules in the molecular formula. It is clearly to know that the central metal ion is bonded to two $C_2O_4^{2-}$ ions, forming a planar molecule, there are two coordinated H_2O molecules perpendicular to the molecular plane [19].

3.3. XRD analysis of all samples

The as-prepared $NiC_2O_4 \cdot 2H_2O$ nanorods were used as the precursor to further synthesis of β-$Ni(OH)_2$, NiO, Ni and nickel complexes nanostructures, as shown in Scheme 1.

The composition and phase purity of the as-obtained samples were characterized by XRD, as shown in Fig. 3A and B. They were confirmed to be pure phases of $NiC_2O_4 \cdot 2H_2O$, β-$Ni(OH)_2$, NiO and Ni in Fig. 3A and a mixture of nickel complexes in Fig. 3B, respectively. Fig. 3A(a) was the orthorhombic $NiC_2O_4 \cdot 2H_2O$ with lattice constants $a = 11.84\,Å$, $b = 5.345\,Å$, and $c = 15.716\,Å$ (JCPDS card No. 25-0582). All of the diffraction peaks in Fig. 3A(b) can be perfectly indexed to the pure hexagonal β-$Ni(OH)_2$ with lattice constants $a = 3130\,Å$ and $c = 4630\,Å$ (JCPDS card No. 74–2075), while those in Fig. 3A(c) were indexed to the hexagonal NiO with lattice constants $a = 3173\,Å$, and $c = 464\,Å$ (JCPDS card No. 89–5881). Fig. 3A(d) was confirmed to be pure cubic Ni with $a = 3.523\,Å$ (JCPDS card No. 87–0712). However, we obtained a mixture of flower-like nickel complexes, which were $[Ni(N_2H_4)_2]C_2O_4 \cdot 5H_2O$ (★, JCPDS card No. 22–1188) and $[Ni(N_2H_4)_3]C_2O_4 \cdot 5H_2O$ (◆, JCPDS card No. 22-1186), confirmed from Fig. 3B. Because of the incomplete conversion, there was still some $NiC_2O_4 \cdot 2H_2O$ precursor (▼) in the nickel complexes sample.

3.4. Discussion of β-$Ni(OH)_2$ and formation mechanism

Fig. 4a–c show the SEM and TEM images of β-$Ni(OH)_2$ prepared under atmosphere condition. The sample is primarily composed of nanorods with diameters of 200 nm and lengths of 1 μm. As shown in Fig. 4b, the β-$Ni(OH)_2$ nanorods are assembled by aggregated hexagonal nanosheets whose side length is 100 nm. Due to the thin hexagonal nanosheets, when they were under long-time bombardment of the electron beam at the accelerating voltage of 200 kV, they began to curve and smashed into many small rods. Therefore, in the TEM image shown in Fig. 4c, we cannot see nanosheets in the β-$Ni(OH)_2$ nanorods [26]. In Fig. 4d, however, the as-synthesized β-$Ni(OH)_2$ was irregular hexagonal morphology prepared under hydrothermal condition. It shows different morphology compared to the product under the atmosphere condition. In addition, their XRD patterns also show slight difference (see Fig. 5) though all the reflectance peaks can be perfectly indexed to β-$Ni(OH)_2$ with lattice

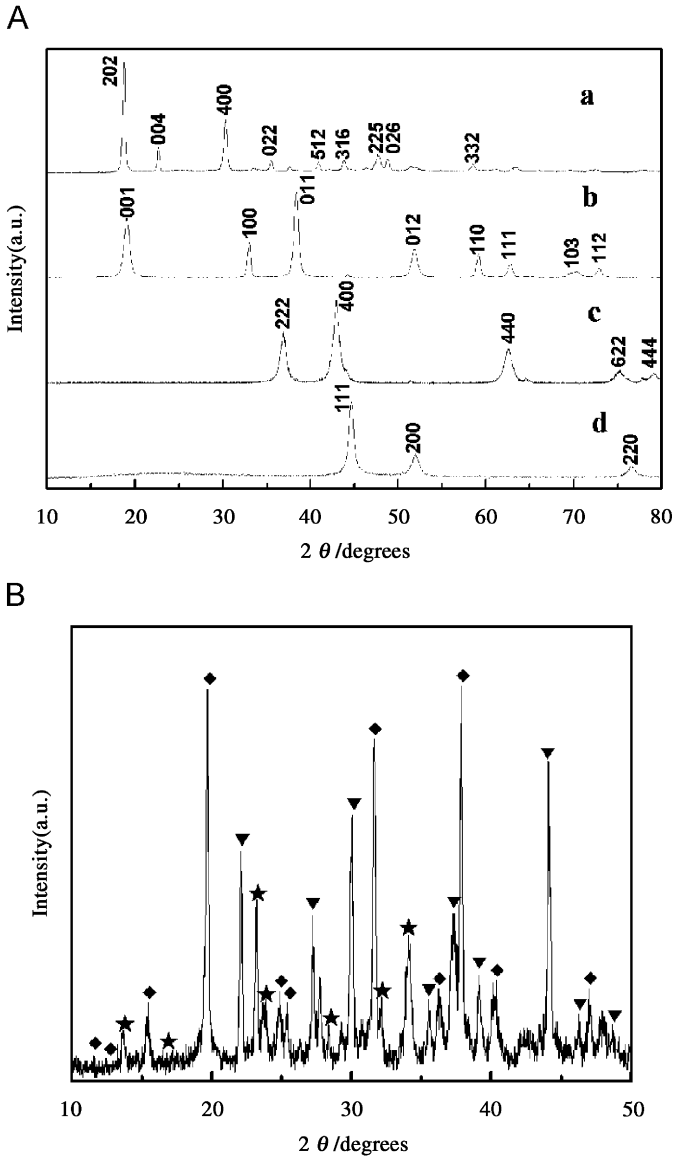

Fig. 3. XRD patterns of all the as-prepared products: (A) (a) $NiC_2O_4 \cdot 2H_2O$ nanorods, (b) β-$Ni(OH)_2$ nanorods, (c) NiO sub-microtubes, (d) Ni nanospheres; (B) flower-like Ni complexes nanostructures $[Ni(N_2H_4)_2]C_2O_4 \cdot 5H_2O$(★), $[Ni(N_2H_4)_3]C_2O_4 \cdot 5H_2O$(●) and $NiC_2O_4 \cdot 2H_2O$(▼) nanorods.

constants $a = 3130$ Å and $c = 4630$ Å (JCPDS card No. 74-2075). The peaks of the product obtained under atmosphere condition are obviously wider than those of the other product, which means the former with smaller diameters.

The $NiC_2O_4 \cdot 2H_2O$ precursor played a very important role and served as a template to form the $Ni(OH)_2$ nanorods and nanosheets. The $C_2O_4^{2-}$ acts as a bidentate ligand in the aqueous solution forming the stable compound. When conversion proceeded in NaOH solution under the hydrothermal condition, the H_2O molecules in the precursor were quickly replaced by OH^-, at the same time the $C_2O_4^{2-}$ ions were gradually substituted by OH^-. Then the plate-like $NiC_2O_4 \cdot 2H_2O$ converted to the $Ni(OH)_2$ nanosheets. Comparing with the method of direct precipitation by the reaction of metal ions and NaOH solution, the rate of the conversion process was much slower. However, the slow substitution of the $C_2O_4^{2-}$ ions can maintain the morphology of the precursor. When $C_2O_4^{2-}$ ions and H_2O molecules are gradually substituted by OH^- ions, there are six OH^- ions coordinating the metal ion Ni^{2+} and forming $Ni(OH)_6$; while one O atom conjugated with three Ni^{2+} ions. Therefore, the resultant molecular formula is $Ni(OH)_2$ and the shape is hexagon. It is the basic building block to construct the hexagonal nanosheets and then assemble the β-$Ni(OH)_2$ nanorods.

3.5. Preparation of other nickel-based nanostructures

The $NiC_2O_4 \cdot 2H_2O$ precursor can also be transferred to other nickel-based nanostructures. Due to the formation of gases, the decomposition of $NiC_2O_4 \cdot 2H_2O$ nanorods leads to the formation of the NiO sub-micortubes. Fig. 6a and b display the SEM and TEM images of NiO, composed of sub-micortubes with diameters of 200 nm and lengths up to 1.5 μm. We can also obtain metallic Ni nanospheres by

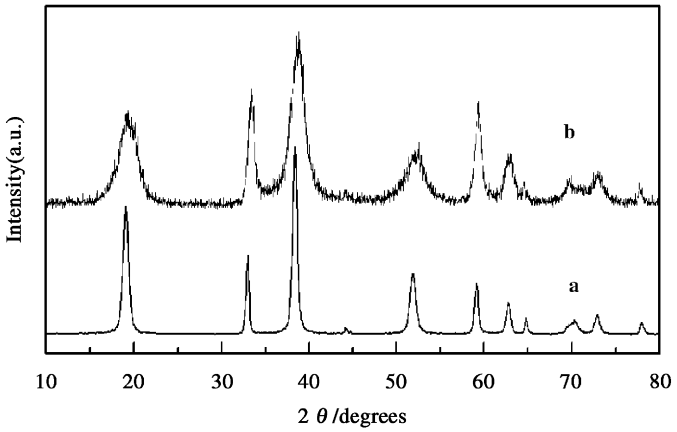

Fig. 5. XRD patterns of β-$Ni(OH)_2$ under different condition: (a) hydrothermal, 100 °C; (b) boiled 100 °C, atmosphere.

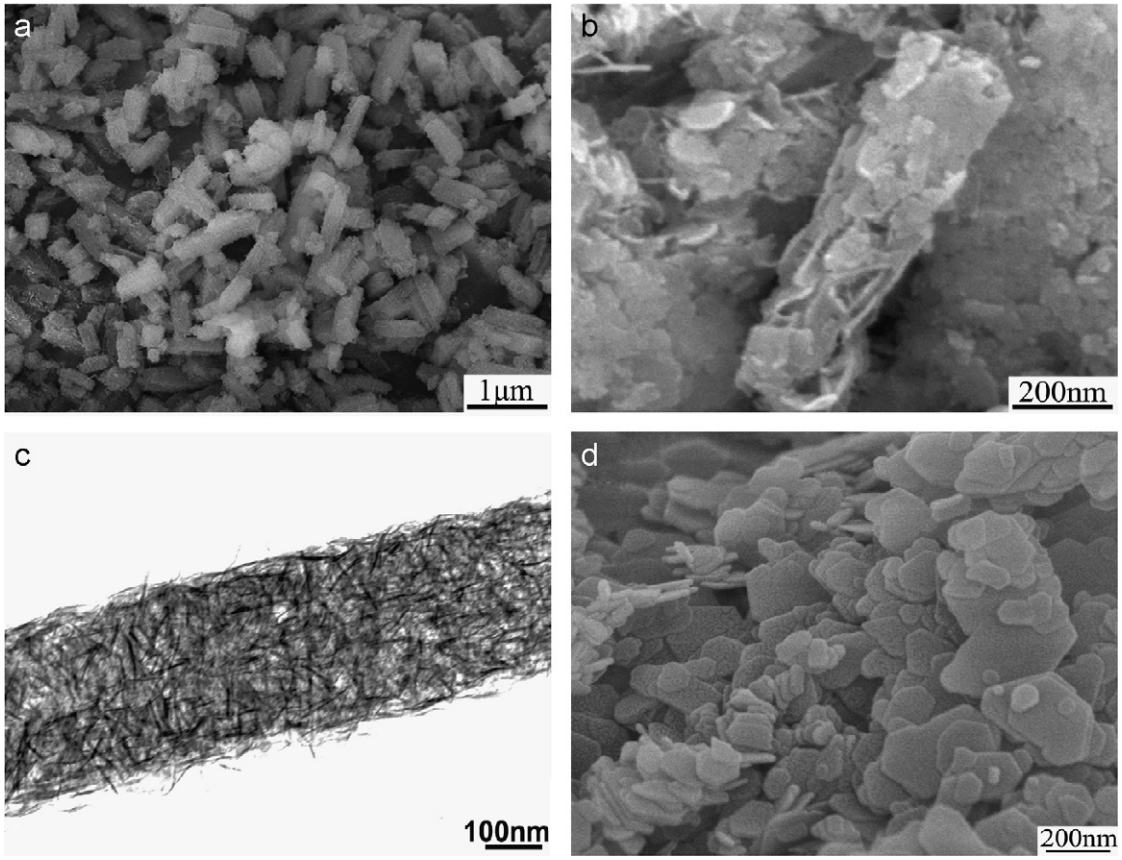

Fig. 4. SEM and TEM images of β-$Ni(OH)_2$ under different conditions: hydrothermal condition (a) SEM image of β-$Ni(OH)_2$; (b) SEM image of one enlarged β-$Ni(OH)_2$ nanorod; (c) TEM image of a β-$Ni(OH)_2$ nanorod; atmosphere condition (d) SEM image of β-$Ni(OH)_2$ nanosheets.

reducing the $NiC_2O_4 \cdot 2H_2O$ precursor with $NH_2NH_2 \cdot H_2O$ under the hydrothermal condition. As shown in Fig. 6c, the diameters of Ni nanospheres were about 300 nm and were polycrystallines inferred from the SAED pattern (inset in 6c), which is well in agreement with the XRD in Fig. 3A(d). Because of the magnetic nature of the Ni nanoparticles, they tend to assemble catenarian morphology, as shown in Fig. 6d.

The flower-like nickel complexes assembled by nanorods were obtained by the reaction of $NiC_2O_4 \cdot 2H_2O$ with $NH_2NH_2 \cdot H_2O$ under an ultrasonic condition, where $NH_2NH_2 \cdot H_2O$ acted as a coordination compound. Fig. 6e and f show the samples with novel and interesting flower-like morphology, and the diameters and lengths of the nanorods were about 200 nm and 1.5–2 μm, respectively, which were coincident with the precursor nanorods.

3.6. Evaluation of the β-Ni(OH)$_2$ electrode

Because of the dense aggregation of the nanosheets in assembling the β-$Ni(OH)_2$ nanorods, there were lesser gaps between the nanosheets but still provide larger surface area (Fig. 4c), it was expected to be a good candidate as an electrode material in rechargeable batteries. The specific capacities of different β-$Ni(OH)_2$ nanostructures have been investigated as anodes, as shown in Fig. 7. Fig. 7a is the β-$Ni(OH)_2$ mircospheres, Fig. 7b is the β-$Ni(OH)_2$ nanorods with nanosheets and Fig. 7c is the β-$Ni(OH)_2$

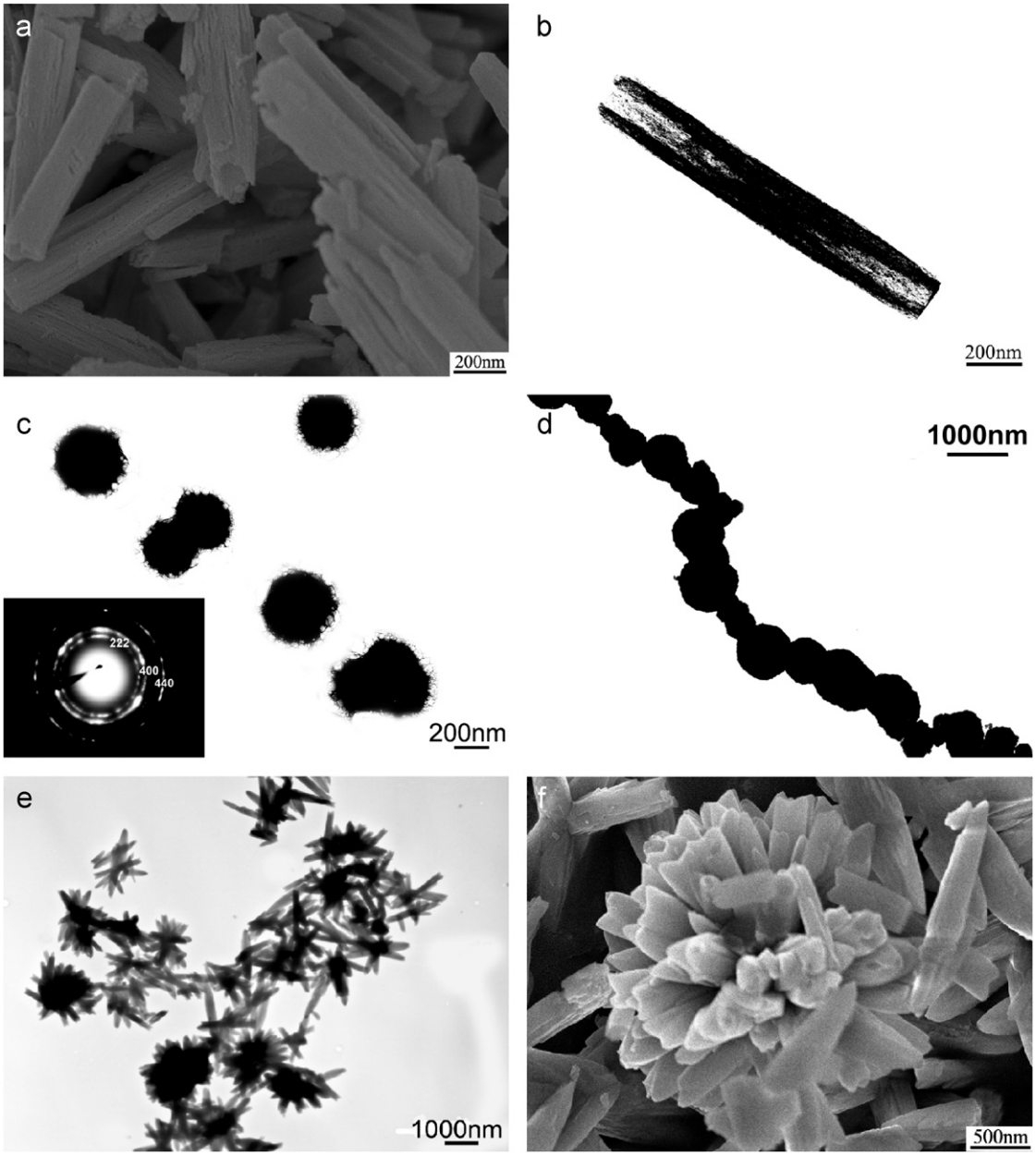

Fig. 6. SEM and TEM images of other nanostructures: (a) SEM and (b) TEM image of NiO sub-microtubes; (c) and (d) are TEM images of Ni nanospheres (inserted is SEAD of (c)); (e) TEM and (f) SEM image of flower-like nickel complexes assembled by nanorods.

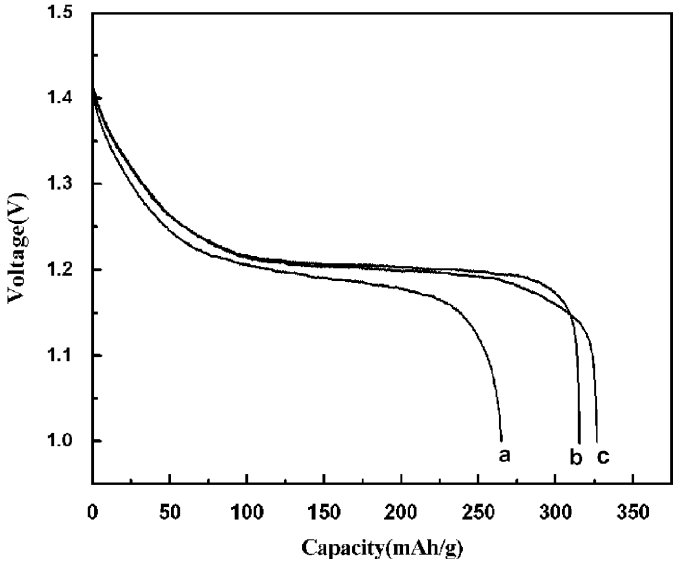

Fig. 7. Discharge curves of β-$Ni(OH)_2$: (a) bulk β-$Ni(OH)_2$; (b) β-$Ni(OH)_2$ nanorods with nanosheets; (c) b dipped with 10% β-CoOOH.

nanorods with nanosheets dipped with 10% β-CoOOH. Their specific capacities are 265.17, 315.27 and 326.81 mAh/g, respectively. It is clearly to see that the capacity of (b) is 18.9% higher than that of (a), while (c) is 3.7% higher than (b), which is consistent with our speculation. It is known that the electrochemical performance of the nickel electrode depends on the proton mobility and the electrical conductivity. The reaction condition to prepare β-$Ni(OH)_2$ nanorods composed of nanosheets led to the improvement of the crystallinity, which reduces the polarization, the increase of the interlayer distance, which is favorable for the diffusion of the proton, and the increase of the proton vacancies, which can improve the proton mobility and electrical conductivity, thus producing materials with high discharge capability [27]. With regard to the much higher specific capacities of the last two β-$Ni(OH)_2$ anodes, which is even higher than that of the theoretical value 289 mAh/g, we assume that there are two possible reasons as followings. First, the high surface activity of the β-$Ni(OH)_2$ nanosheets caused the nickel powders transferred to other active matters. Second, because of the possible uneven polarization, the β-$Ni(OH)_2$ nanosheets transferred to γ-NiOOH which has higher specific capacity. The results suggest that the novel nanostructures will be helpful in improving the electrochemical performance of nickel hydroxide. And if it is dipped solution containing metallic ions such as Al^{3+}, Co^{3+}, Fe^{3+}, Mn^{3+}, Cr^{3+} [27–31], the capacity of β-$Ni(OH)_2$ nanosheets will be further increased.

4. Conclusions

In summary, we have succeeded in controllable synthesis of $NiC_2O_4 \cdot 2H_2O$ nanorod precursor via the microemulsion-mediated solvothermal synthesis method. The morphologies and sizes of the precursor can be readily tuned by adjusting experimental parameters of the reverse micelle/microemulsion system, such as the molar ratio of H_2O to CTAB (defined w), the reaction temperature and time. Furthermore, we have successfully demonstrated that β-$Ni(OH)_2$ nanorods composed of nanosheets, NiO submicrotubes, Ni nanospheres and flower-like nickel complexes assembled by nanorods can be synthesized using the precursor method. This synthetic method is simple and controllable and offers an attractive and convenient path to a large-scale production. We have also investigated the specific capacity of the as-prepared β-$Ni(OH)_2$ nanorods assembled by nanosheets, which suggested their excellent electrochemical performance and potential application in rechargeable batteries. The magnetic properties of NiO sub-microtubes and Ni nanospheres and the catalytic properties of Ni nanospheres are under investigation.

Acknowledgments

This work was supported by the National Natural Science Foundation Council of China (20331010, 20671011, 90406024 and 90406002), the Key Laboratory of Structural Chemistry Foundation (No.060017) and B.Q. Wei thanks the support of the 111 Project (B07012).

References

[1] P. Braos-García, P. Maireles-Torres, E. Rodr'ıguez-Castellón, A. Jiménez-López, J. Mol. Catal. A Chem. 193 (2003) 185–196.
[2] J.Z. Gao, F. Guan, Y.C. Zhao, W. Yang, Y.J. Ma, X.Q. Lu, J.G. Hou, J.W. Kang, Mater. Chem. Phys. 71 (2001) 215–219.
[3] Z.H. Liang, Y.J. Zhu, X.L. Hu, J. Phys. Chem. B 108 (2004) 3488–3491.
[4] T. Seto, H. Akinaga, F. Takano, K. Koga, T. Orii, M. Hirasawa, J. Phys. Chem. B 109 (2005) 13403–13405.
[5] Y.T. Jeon, G.H. Lee, J.H. Park, B. Kim, Y.M. Chang, J. Phys. Chem. B 109 (2005) 12257–12260.
[6] Y.T. Jeon, J.Y. Moon, G.H. Lee, J.H. Park, Y.M. Chang, J. Phys. Chem. B 110 (2006) 1187–1191.
[7] F. Tian, J. Zhu, D. Wei, Y.T. Shen, J. Phys. Chem. B 109 (2005) 14852–14854.
[8] J.C. Bao, C.Y. Tie, Z. Xu, Q.F. Zhou, D. Shen, Q. Ma, Adv. Mater. 13 (2001) 1631–1633.
[9] Y. Morioka, S. Narukawa, T. Itou, J. Power Sources 100 (2001) 107–116.
[10] A. Taniguchi, N. Fujioka, M. Ikoma, A. Ohta, J. Power Sources 100 (2001) 117–124.
[11] A.K. Shukla, S. Venugopalan, B. Hariprakash, J. Power Sources 100 (2001) 125–148.
[12] C. Coudun, J.F. Hochepied, J. Phys. Chem. B 109 (2005) 6069–6074.
[13] D.N. Yang, R.M. Wang, J. Zhang, Z.F. Liu, J. Phys. Chem. B 108 (2004) 7531–7533.
[14] L. Sun, P.C. Searson, C.L. Chien, Appl. Phys. Lett. 79 (2001) 4429–4431.
[15] L. Sun, P.C. Searson, C.L. Chien, Adv. Mater. 17 (2005) 1995–1999.
[16] I.S. Lee, N. Lee, J. Park, B.H. Kim, Y.W. Yi, T. Kim, T.K. Kim, I.H. Lee, S.R. Paik, T. Hyeon, J. Am. Chem. Soc. 128 (2006) 10658–10659.
[17] Y.J. Zhan, C.L. Zheng, Y.K. Liu, G.H. Wang, Mater. Lett. 57 (2003) 3265–3268.
[18] J.H. Yang, L.M. Qi, C.H. Lu, J.M. Ma, H.M. Cheng, Angew. Chem. Int. Ed. 44 (2005) 598–603.
[19] X.L. Li, J.F. Liu, Y.D. Li, Mater. Chem. Phys. 80 (2003) 222–227.

[20] C.K. Xu, K.Q. Hong, S. Liu, G.H. Wang, X.N. Zhao, J. Cryst. Growth 255 (2003) 308–312.
[21] M.H. Cao, C.W. Hu, E.B. Wang, J. Am. Chem. Soc. 125 (2003) 11196–11197.
[22] M.H. Cao, Y.H. Wang, C.X. Guo, Y.J. Qi, C.W. Hu, Langmuir 20 (2004) 4784–4786.
[23] M.H. Cao, Y.H. Wang, Y.J. Qi, C.X. Guo, C.W. Hu, J. Solid State Chem. 177 (2004) 2205–2209.
[24] M.H. Cao, X.L. Wu, X.Y. He, C.W. Hu, Langmuir 21 (2005) 6093–6096.
[25] L.N. Sun, Q.R. Guo, X.L. Wu, S.J. Luo, W.L. Pan, K.L. Huang, J.F. Lu, L. Ren, M.H. Cao, C.W. Hu, J. Phys. Chem. C 111 (2007) 532–537.
[26] G.B. Sun, M.H. Cao, Y.H. Wang, C.W. Hu, L. Ren, K.L. Huang, Chem. Commun. (2005) 1740–1742.
[27] H.B. Liu, L. Xiang, Y. Jin, Cryst. Growth Des. 6 (2006) 283–286.
[28] C. Faure, C. Delmas, P. Willmann, J. Power Sources 36 (1991) 497–506.
[29] L. Demourgues-Guerlou, C. Delmas, J. Power Sources 45 (1993) 281–289.
[30] L. Indira, M. Dixit, P.V. Kamath, J. Power Sources 52 (1994) 93–97.
[31] L. Demourgues-Guerlou, C. Delmas, J. Power Sources 52 (1994) 275–281.